Kuwait J. Sci. Eng. **34** (2A) pp. 91-109, 2007

An iterative technique to estimate baseline parameters in SAR interferometry

RAO, K. S.[1], BHAGAVATH K. P[2]., VISHAL[2] AND AL JASSAR, H. K.[1]

[1]*Physics Department, Faculty of Sciences, Kuwait University, Kuwait. P.O.Box 5969*

[2]*Civil Engineering Department, Indian Institute of Technology, Roorkee, India.*

ABSTRACT

Baseline, the shortest distance between two satellite trajectories, is an important parameter in Synthetic Aperture Radar Interferometry as it has direct impact on the accuracy of Digital Elevation Models and surface displacement measurements due to land subsidence, earthquake etc. Exact and simplified models for the estimation of baseline parameters for a flat earth as well as a curved earth were developed. The results are compared with the existing simplified models and found to be in good agreement. The baseline parameters are estimated using a Newton-Raphson method followed by a least square technique by simulating 90 ground control points which were well distributed all over the satellite scene (heights - phases). The interferogram phases were corrupted with various types and levels of phase noise. An iterative technique for the improvement of baseline estimation by minimizing the phase noise is illustrated with examples. A transformation function is developed to reduce the phase noise of the rest of the image for generating a DEM.

Keywords: baseline parameters, digital elevation models, microwave remote sensing, phase noise, SAR interferometry, simulations, statistical techniques, surface deformation.

INTRODUCTION

SAR interferometry (InSAR) is a remote sensing technique which finds applications in various fields such as Digital Elevation Models (DEMs) generation, land subsidence mapping, surface displacement due to earthquakes, monitoring of volcanoes, estimation of glacier movement and run-off, monitoring of land slides etc. The concept of this technique is to interfere the phases of two complex SAR images of the same scene (by registering them with an accuracy of a fraction of a pixel), but acquired from different orbits by the same satellite (or different satellites with the same configuration). The interferograms thus obtained will be unwrapped and then transformed in terms

of surface displacement or elevations of the ground or the flow of glaciers as per the context. Further details on the InSAR technique can be seen in the references (Zebker and Goldstein 1986, Bamler 1998, Indian InSAR group 1999, Massonnet *et al.* 1993, Hanssen 2001).

The InSAR technique is a cost effective approach (Toutin and Gray, 2000) for generating DEM of high spatial ($\approx$ 20 m) and vertical ($\approx$5 m) accuracy. Recently, efforts have been underway to further improve the vertical accuracy of the DEM generated through an InSAR technique (Small & Nüesch 1996, Seymour & Cumming 1996, Kumar 2001,). The Shuttle Radar Topography Mission (SRTM) is a special effort in this direction (Stefan *et al.*, 2000). The vertical accuracy of an InSAR derived DEM mainly depends on the accuracy of the baseline estimation (Li & Goldstein 1990, Abdelfattah *et al.*, 2000) and the degree of phase noise. Baseline is defined as the shortest distance between two satellite tracks (at the InSAR position) from which the two images are taken. It has vertical and horizontal components. The baseline parameters often referred in this paper are as follows (refer to Figure 1):

B -- Baseline, the minimum distance between the two satellite trajectories,

B_v -- Vertical component of baseline with reference to horizontal plane,

B_h-- Horizontal component of baseline with reference to horizontal plane,

$B_\perp$ - Perpendicular component of the baseline with reference to slant range,

$B_{//}$ – Parallel component of the baseline with reference to slant range,

dB_h, dB_v, $dB_\perp$ are the variation in baseline along azimuth (per 100 km.),

C - Phase constant with respect to the datum level, and

h_a - Elevation corresponding to 2π phase in an interferogram after flat earth fringes are removed (ambiguity height).

There are several methods for the estimation of baseline parameters. To mention a few:

- Precision orbit approach (Small *et al.* 1993),
- Ground Control Points (GCP) approach (Seymour & Cumming 1996),
- Flattened terrain interferometric fringes approach (Prati & Rocca 1990, Singh *et al.* 1997), and
- Corner Reflectors approach (Prati *et al.*, 1993).

Each method has its own advantages/disadvantages under given conditions. For example, the Corner Reflectors approach needs preplanning and installation of the reflectors synchronously with the satellite passes. The

flattened terrain interferometric fringe approach is very useful in gently undulating terrain with the least vegetation cover, particularly desert-like landscapes. A GCP approach needs precise measurement of elevations and identification of their locations in the intensity images to a sub-pixel accuracy. One should choose the regions of high coherence for the control points so that the effect of phase noise can be minimized. Also, it is preferable that the GCP location can be such that the same features should extend for at least 3 x 3 pixels with reasonably flat terrain. This can be easily achieved and will ensure the correctness of GCP. The precision orbit approach is the simplest but needs very precise knowledge on the satellite trajectories which generally are not accessible to every user.

It can be seen from the literature (Knedlik *et al.*, 1999, Wu *et al.*, 2002) that most of the authors used a GCP approach for the estimation of baseline parameters due to its high accuracy. The commercial SAR Interferometry software packages (for example GAMMA interferometry software) also uses a GCP approach.

Knedlik *et al.* (1999) made a detailed analysis on the accuracy of estimation of baseline using Kalman filter and varying baseline from 50 to 1130 m. They reported an error of -0.53 to 2.32 m in B_h and -0.66 to 0.89 m in B_v. Larger errors were reported at a lower baseline. However, the baseline estimation error as a function of phase noise was not carried out. Wu *et al.* (2002) studied the accuracy of estimation of $B_\perp$ by simulating 100 levels of phase noise in the range 0 - 20%. They suggested a transformation function to reduce the effect of phase noise.

In this paper, the authors have adopted the GCP approach for the estimation of baseline parameters. The error in the estimation of baseline was investigated as a function of degree of phase noise and baseline length. In the subsequent sections, derivation of the exact model, reduction to a simplified model, inversion method for the estimation of baseline parameters, the simulation of various levels of phase noise, an iterative technique to reduce the effect of noise on baseline estimation and a transformation function to correct the phase image for generating DEM by reducing the noise etc. are discussed.

RELATION BETWEEN INTERFEROMETRIC PHASE, HEIGHT AND BASELINE PARAMETERS

Derivation of exact model for phase - height - baseline relationship

The standard geometry of a SAR interferometric system in the plane orthogonal to the azimuth direction is shown in Fig. 1 (Fig. 1a for flat earth and Fig. 1b for curved earth). $S_1$and S_2 are two satellite positions separated by a baseline B

having an angle α with the horizontal plane. Let the image taken by S_1 be the master (reference image) and that of S_2 be the slave image (to be re-sampled to register with S_1). The origin of the coordinate system is at S_1. Let us consider two points P_1 and P_2 located in the image at a heights 0 and h meters with respect to a reference surface. The difference in the ranges of P_1 and P_2 from S_1 is partly due to the horizontal and partly due to the vertical component of the range difference. Since we are interested in developing a model to establish the relation between height and phase, we will consider the range difference (phase) only due to the vertical range difference and not the horizontal range difference. In this case, the ranges of P_1 and P_2 from S_1 will be the same, i.e,. θ and $\partial\theta$ are the incident angle and the change in the incident angle, respectively, as shown in Figs. 1a and 1b. The coordinates of S_2, P_1 and P_2 can be shown as (B_h, B_v), (r sinθ, - r cosθ) and (r sin ($\theta + \partial\theta$), - r cos ($\theta + \partial\theta$)) respectively.

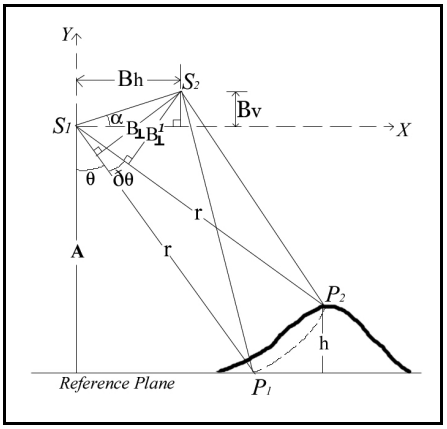

Figure 1a. SAR Interferometry geometry for flat earth model

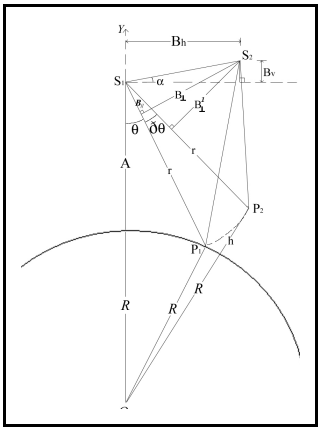

Figure 1b. SAR Interferometry geometry for curved earth model

The path difference δ is given by

$$\delta = 2[(S_1P_2 - S_2P_2)-(S_1P_1 - S_2P_1)] = 2[(r-S_2P_2)-(r-S_2P_1)] = -2[S_2P_2-S_2P_1]$$

Using the distance formula, we can calculate:

$$S_2P_1 = \sqrt{(B_h - r\sin\theta)^2+(B_v + r\cos\theta)^2} \text{ and}$$

$$S_2P_2 = \sqrt{(B_h - r\sin(\theta+\partial\theta))^2+(B_v + r\cos(\theta+\partial\theta))^2}$$

The interferometric phase, $\varphi = \frac{2\pi}{\lambda}\delta$.

Therefore,

$$\varphi = -(4\pi/\lambda)[\sqrt{(B_h - r\sin(\theta+\partial\theta))^2+(B_v + r\cos(\theta+\partial\theta))^2} - \sqrt{(B_h - r\sin\theta)^2+(B_v + r\cos\theta)^2}] \quad (1)$$

Case 1. For flat earth with A as the altitude of the satellite ;

r = A/cos θ and

cos $(\theta + \partial\theta)$ = (A−h)/r = (1-h /A) cosθ.

Case 2. For curved earth with radius R (as shown in Fig. 1b):

$r = (R+A)\cos\theta - \sqrt{R^2 - (R+A)^2\sin^2\theta}$ and

$$(\theta + \partial\theta) = \frac{r^2+(R+A)^2-(R+h)^2}{2r(R+A)}.$$

Equations for curved earth can be reduced to flat earth as R tends to infinity. Since equation 1 is non-linear, the height for a given phase can be estimated using Newton - Raphson technique followed by a least square method.

Simplification of exact model

The details of all the derivations presented can be seen from Bhagavath and Vishal (2002). It can be easily seen from Figs. 1a and 1b, that

$B_h = B\cos\alpha$, $B_v = B\sin\alpha$,

$B_\perp = B_h\cos\theta + B_v\sin\theta$ and $B_{||} = B_h\sin\theta - B_v\cos\theta$

Considering only S_2P_1:

$$S_2P_1 = \sqrt{(B_h - r\sin\theta)^2+(B_v + r\cos\theta)^2} = \sqrt{[r - B_{\iota\iota}]^2+B_\perp^2},$$

$S_2P_1 \approx (r - B_{\iota\iota})\left[1 + \frac{1}{2}\left(\frac{B_\perp}{r-B_{\iota\iota}}\right)^2\right]$ (using Binomial expansion and truncating the higher terms) and $S_2P_1 \approx r - B_{\iota\iota} + \frac{B_\perp^2}{2r}$ (by neglecting $B_{\iota\iota}$ compared to r).

Similarly, we can calculate $S_2P_2 = r - B^1_{\iota\iota} + \frac{B^1_\perp{}^2}{2r}$

where $B^1_{\iota\iota}$ and $B^1_\perp$ are the components of baseline resolved along and across S_1P_2

$B^1_{\iota\iota} = B\sin(\theta - \alpha + \partial\theta = B[\sin(\theta-\alpha)\cos\partial\theta + \cos(\theta-\alpha)\sin\partial\theta] = B_{\iota\iota} + B_\perp\partial\theta$ (since $\partial\theta$ is small).

Similarly $B^1_\perp = B\cos(\theta - \alpha + \partial\theta) = B_\perp - B_{\iota\iota}\partial\theta$

Now the phase difference can be represented as:

$$\varphi = \frac{4\pi}{\lambda}\left[B_{\iota\iota} - B^1_{\iota\iota} + \frac{\left(B^1_{\perp}2 - B^2_{\perp}\right)}{2r}\right]$$

$$= \frac{4\pi}{\lambda}\left[-B_{\perp}\left(1 + \frac{B_{\iota\iota}}{r}\right)\partial\theta\right] \text{(neglecting } \partial\theta^2 \text{ terms).}$$

Case 1: Flat earth: $\partial\theta = \frac{h}{A\tan(\theta)}$.

Hence we have,

$$h = \frac{\lambda A \tan\theta}{4\pi B_{\perp}\left(1 + \frac{B_{\iota\iota}}{r}\right)}\varphi \tag{2}$$

Since $B_{\iota\iota} << r$, neglecting $\frac{B_{\iota\iota}}{r}$, the above formula reduces to Franceschetti & Lanari (1999).

Case 2: Curved earth: $\partial\theta = \frac{h}{K\tan\theta}$ where $K = \left[\frac{(R+A)^2 + r^2 - R^2}{2R}\right]$.

So we have,

$$h = \frac{\lambda K \tan\theta}{4\pi B_{\perp}\left(1 + \frac{B_{\iota\iota}}{r}\right)}\varphi \tag{3}$$

COMPARISON OF DIFFERENT MODELS

There are several simplified models for the conversion of phase to height (Wu *et al* 2002). The models derived by Franceschetti & Lanari (1999) and Massonnet & Feigl (1998) and our model (Equation 2) are compared as a function of baseline and range. For the sake of completeness, the models of Franceschetti & Lanari and Massonnet & Feigl are reproduced here:

Franceschetti & Lanari model: $h = \frac{\lambda r \sin\theta}{4\pi B_{\perp}}\varphi$.

Massonnet & Feigl model: $h_a = [\lambda R_s (\tan(g_i)\cos(\theta) - \sin(\theta))] / (2\delta)$.

The meaning of different terms in the above expressions can be seen in the respective papers. For the convenience of comparison, a new parameter h_a, ambiguity height, is defined as the height for one fringe. All the four models are programmed and the results are computed. Fig. 2a shows h_a as a function of $B_{\perp}$ at middle range. It can be seen from Figure. 2a that as the $B_{\perp}$ increases, h_a decreases. At lower $B_{\perp}$, there is a large variation in h_a in different models, whereas the difference decreases as the $B_{\perp}$ increases. For example at $B_{\perp} = 100$ m, the h_a values are 90.6, 107.3 and 109.8 m respectively for Massonnet & Feigl, Franceschetti & Lanari, our simplified model for flat earth, and exact model.

Figure 2b shows h_a as a function of incidence angle for 100 m $B_\perp$. It can be seen from Fig. 2b that as incidence angle increases, h_a increases. The exact model gives higher h_a compared to the simplified models. The curved earth model gives a higher $h_a$compared to flat earth (Fig. 2d). The h_a given by simplified curved earth model and exact model differ by only 2.48 m and this decreases with increasing $B_\perp$. For $B_\perp$ above 200 m, practically there is no difference among the models.

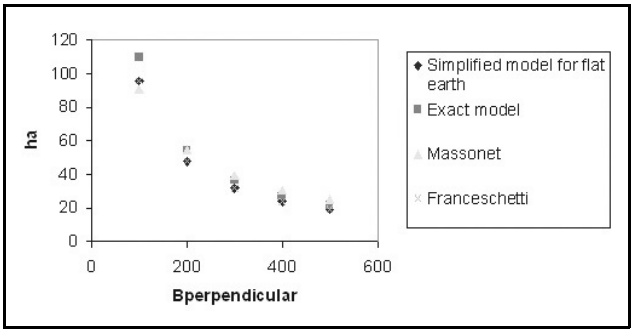

Figure 2a. Comparison of different models as a function of Bperpendicular

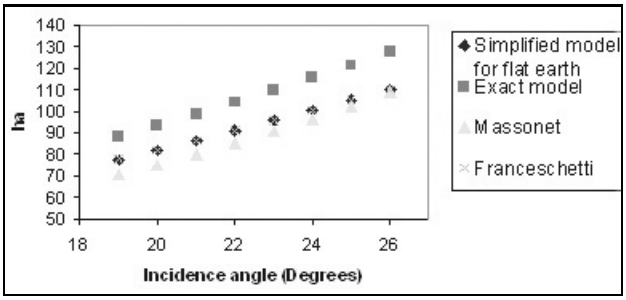

Figure 2b. Comparison of different models as a function of Incidence angle

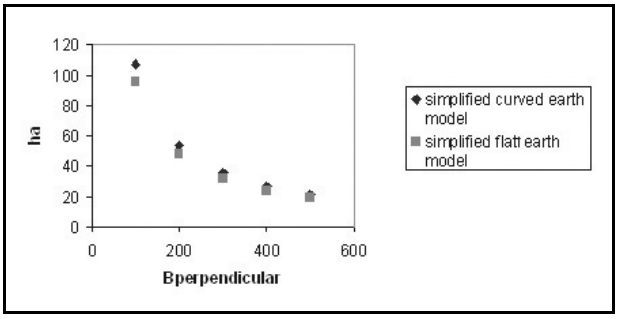

Figure 2c. Comparison of flat and curved earth simplified models as a function of Bperpendicular

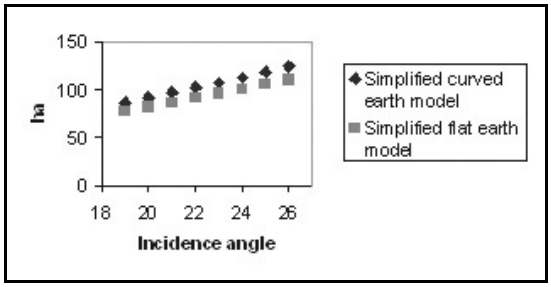

Figure 2d. Comparison of Flat and curved earth simplified models as a function of incidence angle

A MODEL FOR THE ESTIMATION OF BASELINE PARAMETERS

Simulation of control points

A set of 90 GCPs is simulated (10 in the azimuth x 9 in the range direction at equal intervals) for a scene of 100 x 100 km of SAR. A random terrain model is used to generate DEM in the range of 0 to 100 m elevations. Figure 3a shows representative elevation profiles in the range and azimuth directions. Out of 90 GCPs, 20 GCPs are randomly selected for testing the model. Figures 3b & c shows the distribution of GCPs for 90 and randomly selected 20 points, respectively.

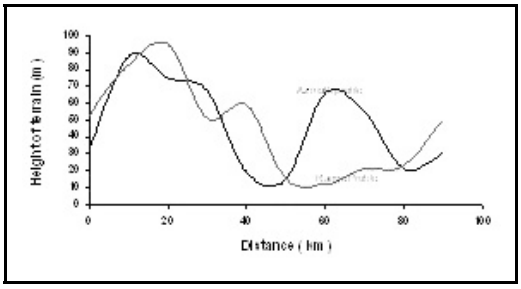

Figure 3a. A typical elevation profile in the range and azimuth directions

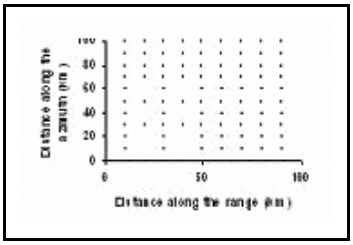

Figure 3b. The distribution of 90 GCPs in ERS scence of 100 x 100 km.

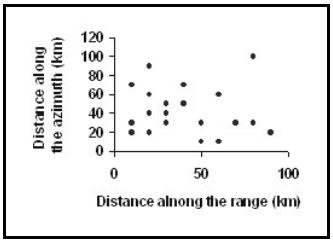

Figure 3c. The distribution of randomly selected 20 GCPs in ERS scene - One case study.

Estimation of baseline parameters

Since $B_\perp$ and $B_{||}$ vary with range, it is appropriate to resolve them with reference to the horizontal plane, i.e., B_h and B_v. From the study of different data sets over India (as given in Table 1), we observed a variation of 2 - 20 m in $B_\perp$ along azimuth for 100 km. Therefore, the baseline parameters estimated are B_h, B_v, dB_h, dB_v and C as explained in the introduction.

Table 1: Variation of baseline perpendicular at various places in India

Site Name	Start Line $B_\perp$	End line $B_\perp$	Difference
Chamoli	70.0	73.2	-3.2
Kolar	105.6	111.3	-5.7
Bankura	171.1	163.1	8.0
Bhuj	163.3	156.6	6.7
Koyna (pair-1)	121.0	115.9	5.1
Koyna(pair-2)	150.7	146.0	4.7
Bombay	126.2	124.3	1.9
Latur (pair-1)	17.0	36.0	-19.0
Latur (pair-2)	34.0	54.0	-20.0

The exact equation is used for the estimation of baseline parameters by replacing B_v with $B_v + n.dB_v$ and B_h with $B_h + n.dB_h$ where n is the ratio of azimuth line number to the total number of lines in the100 km scene along the azimuth is:

$$F = -2[\sqrt{(B_h + ndB_h - r\sin(\theta + \partial\theta))^2 + (B_v + ndB_v + r\cos(\theta + \partial\theta))^2}$$

$$-\sqrt{(B_h + ndB_h - r\sin(\theta))^2 + (B_v + ndB_v + r\cos(\theta))^2}] + C -- \delta$$

For 90 and 20 GCPs, the phase values are simulated using above equation suitable for ERS SAR data.

Newton-Raphson numerical technique

Since the above equation is non-linear in h, it can be easily solved using the Newton-Raphson iterative technique by finding the differentials of the parameters. Thus, the iterative equations for the Newton- Raphson Technique are:

$$F_{ij} + \left(\frac{\partial F}{\partial B_h}\right)_{ij} k + \left(\frac{\partial F}{\partial dB_h}\right)_{ij} l + \left(\frac{\partial F}{\partial B_v}\right)_{ij} p + \left(\frac{\partial F}{\partial dB_v}\right)_{ij} q + \left(\frac{\partial F}{\partial C}\right)_{ij} t = 0, \text{ where}$$

'i' is the iteration number, and 'j' = 1,2,3..... n, no. of GCPs.

Any initial values of B_h, B_v, dB_h, dB_v & C are assumed and the value of the above equations are calculated for i = 0^{th} iteration. Now, the 'n' (= 90 or 20) linear equations for five variables are solved using the least square method. For other iterations, the values of the above parameters are updated as:

$$B_h^{i+1} = B_h^i + k, \quad dB_h^{i+1} = dB_h^i + l,$$

$$B_v^{i+1} = B_v^i + p, \quad dB_v^{i+1} = dB_v^i + q, \text{ and } C^{i+1} = C^i + t\,.$$

This iterative process is continued until the values B_h, B_v, dB_h, dB_v & C converge within a given threshold. It has been noticed that the above method is very powerful and it converges within 2-3 iterations. Table 2 gives errors in the estimation of baseline parameters for different baselines. It can be seen from Table 2 that the errors are within a few mm. Christoph et. al (1996) has indicated in his paper the requirement of an accuracy of 5 cm in the estimation of baseline. This proves the validity of our inversion approach.

Table 2: Error (cm) in the estimation of baseline parameters for zero phase noise different Baselines

Parameter	B = 100	B = 200	B = 300
B_h	-0.0400	-0.1000	0.100
dB_h	0.0640	0.2250	0.040
B_v	0.1100	0.2700	-0.140
dB_v	-0.1480	-0.5200	-0.020
C	0.0000	0.0000	0.000

A STUDY ON THE STABILITY OF THE MODEL VS. PHASE NOISE

It may be noted that the results reported in Table 2 are free from phase noise. Generally the interferometric phase values are corrupted by system noise and the noise due to target variability (Zebker & Villasenor, 1992). The system phase noise will be of the order of 0.6 radians of phase (equivalent to 5 m error in DEM). In repeat pass interferometry, the two scenes are acquired at different times. During this period, there may be changes in the terrain such as vegetation cover, forest growth and soil moisture levels which cause temporal de-correlation of the phase signal. This will be reflected in the coherence image. Therefore one has to study the stability of estimation technique against phase noise. For this purpose, different levels of phase noise are simulated and the model has been thoroughly tested.

Simulation of phase noise

Different models used for the simulation of phase noise as illustrated in Fig. 4 include unweighted random noise, weighted (Gaussian) random noise, percentage random Gaussian noise, positively biased, negatively biased and unbiased noise etc. All the models are implemented and investigated in this paper. However, the results of percentage random Gaussian noise distribution are reported here. Please refer to the report by Bhagavath and Vishal (2002) for results on the different types of phase noise. A representative histogram of simulated noise is shown in Fig. 5a at noise level of 20% (for Gaussian random distribution of noise) and Fig. 5b at noise level of 10% (for unweighted positively biased random distribution of noise) by simulating 200 random combinations for 90 GCPs.

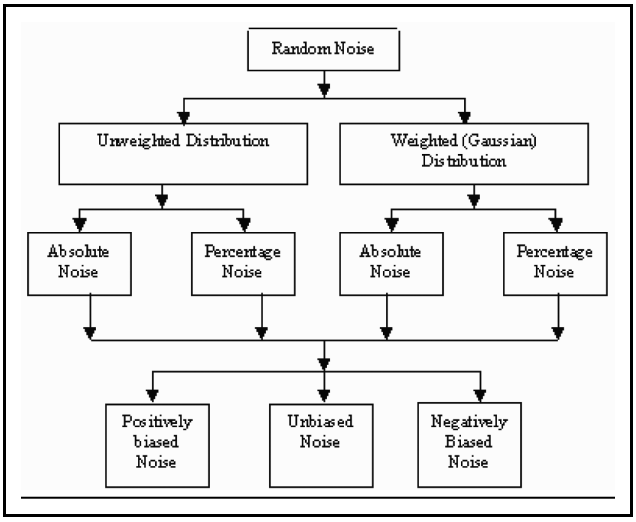

Figure 4. Simulation of different types of random distribution of phases

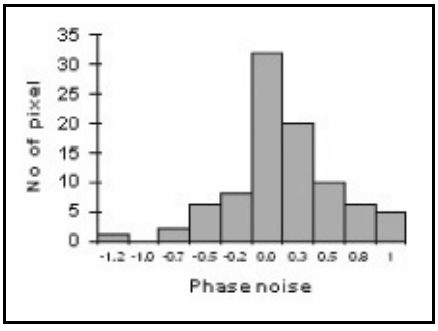

Figure 5a. Histogram of 20% random Gaussian noise with zero mean

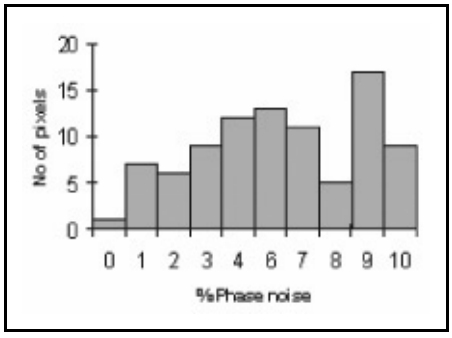

Figure 5b. Histogram of 10% unweighted noise

Estimation of baseline with noise

Using the methodology explained earlier, the baseline parameters B_h, B_v, dB_h, dB_v &C are estimated using the noisy phase data. Figures 6a, b and c show the errors in $B_\perp$ as a function of percentage random Gaussian noise. Two hundred sets of noise levels are simulated in the range of 0% to 20% to represent the above Figs. It can be seen from Fig. 6 that the errors in the estimation of $B_\perp$ linearly increase with the noise level. For example, the error in the estimation of $B_\perp$ for 20% positively biased Gaussian random noise varies from 6 to 14 m depending on the random combination of the phase noise (see Fig. 6b). Figure 7 shows a linear relation between the RMS error in the estimation of $B_\perp$ and % noise level. Similar results are reported by Wu (2002) for a different system parameter.

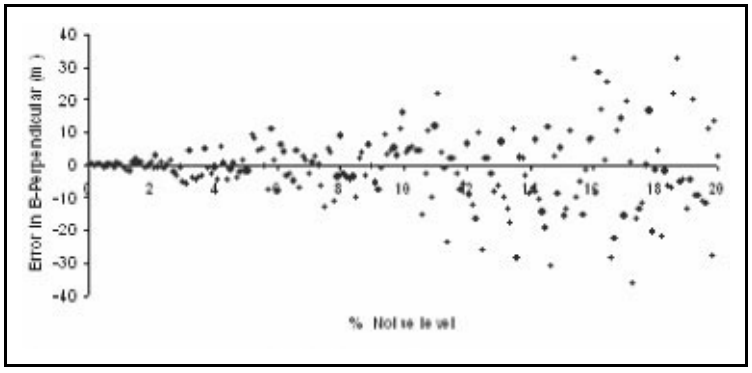

Figure 6a. Error in the estimation of B-perpendicular for understanding Gaussian random distribution. N0. of GCPs = 20, B = 200 m.

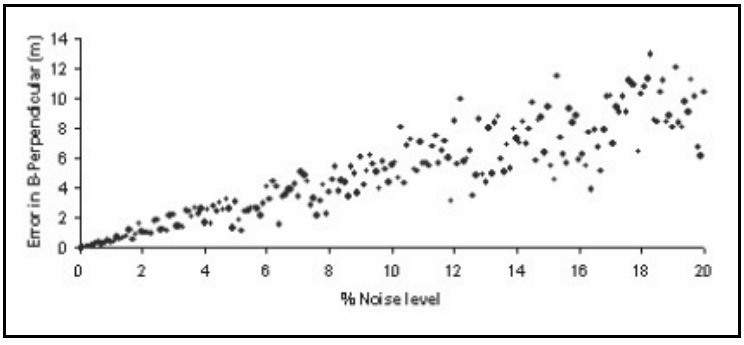

Figure 6b. Error in the estimation of B-perpendicular for positively biased Gaussian random distribution. Number of GCPs 9, B = 100 m,

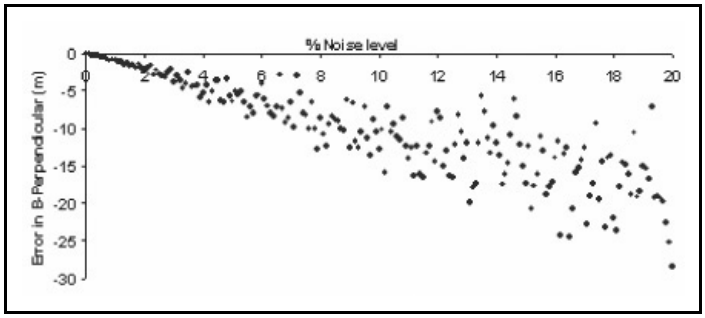

Figure 6c. Error in the estimation of B-perpendicular for negatively biased Gaussian random distribution. No. ofGCPs = 90, B = 200 m.

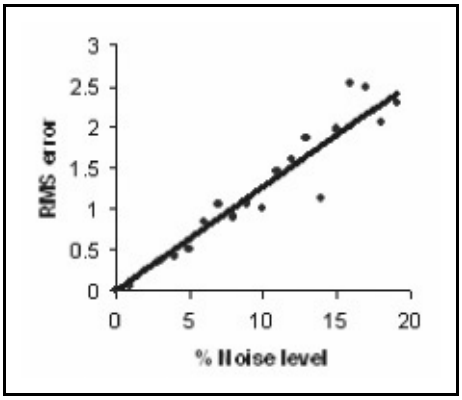

Figure 7. RMS error of B-Perpendicular for 90 GCPs & 200 phase noise simulations

An iterative technique to minimize the effect of noise on baseline estimation

As per the discussion in earlier Sections, the phase noise introduces error in the estimation of baseline parameters. Therefore there is a need to minimize the phase noise before it is used for the baseline estimation. There are several filtering techniques to reduce the noise in the data. For example, the coherence image can be taken as a reference for designing a weighted filter to reduce phase noise. It is difficult to simulate a coherence image and in the absence of such information, an iterative method is proposed. The steps are as follows:

Estimate the baseline with the noisy phase data as described eralier:

$B = N(\Phi)$ (Fig. 6).

Using the above baseline and the exact model, back calculate phases:

$\Phi' = F(B)$ (Equation 1).

Find the error in the phases and then draw a graph between modulus of phase errors vs. initial phase values:

$\Delta\phi \quad = (\phi - \phi')$.

Find the line of best fit of the above data and estimate the coefficients (slope a_0 and intercept a_1):

$\hat{a}_0$ and $\hat{a}_1$ (Fig. 8) .

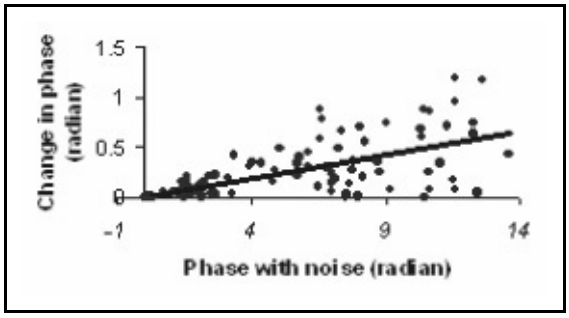

Figure 8. A comparison of the estimated phase noise for iteraction 1 as a function of phase corrupted with 20% noise. The line shows the best fit.

Update the phases with the estimated noise levels:

$|\Delta\phi'| = a_0\phi + a_1$ and $\phi'' = \phi$ - $|\Delta\phi'|$* sign $(\Delta\phi)$

Repeat steps (a) to (e) using updated phase values.

End the iteration when the estimated phase noise converges to a constant value or minimum noise (Fig. 9). The iterations always leads to convergence as explained below:

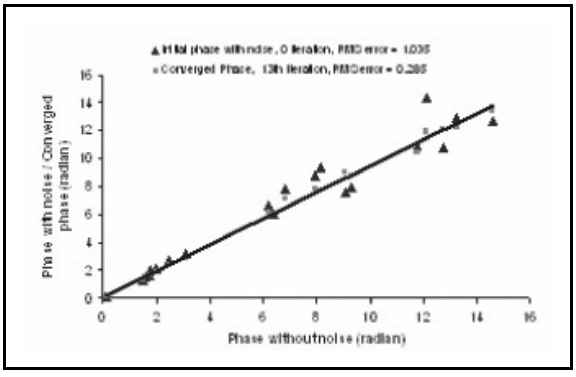

Figure 9. Minimization of phase noise through iterative technique. No. of GPS = 20, B = 200 m., noise level = 20%. The line represents the best fit with converged data.

The first iteration produces more error in the estimation of baseline parameters due to noisy phase data. As the phases are updated to reduce the noise, the estimated baseline parameters for the second iteration will be better than the first iteration. Thus as the iteration number increases, the phase noise converges to mean value and thereby increases the accuracy of estimation of baseline parameters.

Figure 10 shows the improvement in the estimation of baseline parameters with iteration number. For example, the initial estimate of $B_\perp$ for 20% noise is 110.65 m whereas the actual value is 100.2 m. $B_\perp$ converged to 104.88 m after 15 iterations. Therefore, an improvement of 5.77 m of $B_\perp$ has been achieved for 20% noise level. The errors in the estimation of baseline as reported by Knedlik *et al.* (1999) varies from -0.84 to 2.2 m for the estimation of $B_\perp$ with a certain level of noise in phase. A similar level of improvement is seen for 5% noise (the error in $B_\perp$ reduces from -2.14 to -0.44 m in 15 iterations as can be seen from Fig. 10a). The RMS error (Fig. 10b) decreased from 0.49 to 0.09, which shows a considerable improvement.

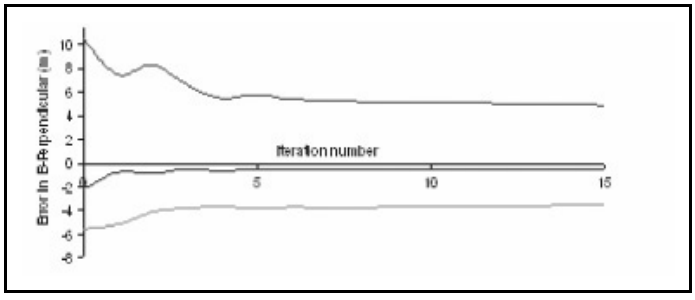

Figure 10a. Improvement in the estimation of B-perpendicular with iteration. No. of GCPs = 90, B = 100 m.

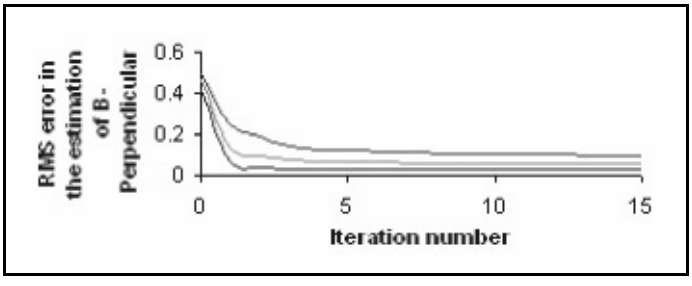

Figure 10b. Improvement in the standard deviation for the estimation of B-perpendicular with iteration. No. of GCPs = 90, B = 100 m.

Generating DEM

The phase noise of the entire image needs to be minimized before generating DEM using the exact curved earth model. For this purpose, a transformation function is developed. The coefficients of the curve (usually second degree polynomial) of best fit between the initial phase values and the converged final phase values are estimated. The phase values of the entire image has to be modified using these coefficients to minimize the noise levels and thereby achieve high accuracy of the DEM. To illustrate this point, the phases of 90 GCPs are corrupted with 20% noise level and the GCPs are made into two groups, each with 45 GCPs by random selection. The transformation coefficients are estimated using the first set of 45 GCPs (Fig. 11). The corrected phase is $-0.0565x^2 + 1.3782x - 0.2599$ where x is phase with noise. The coefficients are data dependent and these coefficients are used to correct the phases of the second set of 45 GCPs. The RMS error of phase noise reduced from 0.45 to 0.27 with the help of the transformation function. Similarly the $B_\perp$ estimation is improved from 117.88 to 111.04 m whereas the correct value is 100.2 m.

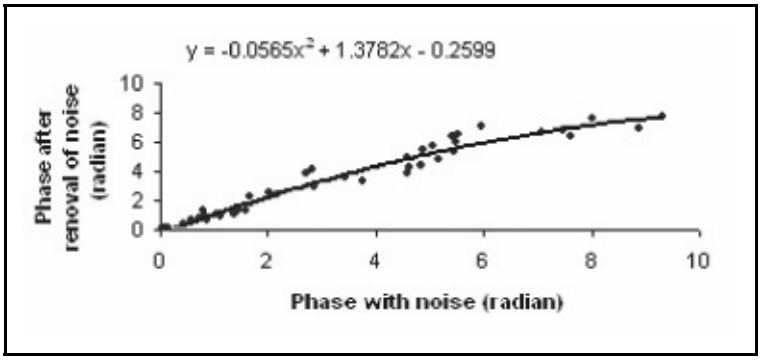

Figure 11. The noisy phase needs to be filtered using the transformation function The curve shown is the best fit for a two degree polynomial.

CONCLUSIONS

The simplified models developed here are comparable with the existing models. At lower $B_\perp$, there is a large variation in h_a in different models whereas the difference decreases as the $B_\perp$ increases. The curved earth model gives higher h_a values and above a 200m baseline, there is practically no difference between flat earth and curved earth models. The baseline parameters are estimated to an accuracy of a few mm in the absence of phase noise. The authors are able to show how the phase noise affects the estimation of baseline parameters using GCPs. An iterative approach is suggested to find the transformation coefficients

to reduce the random noise in the GCPs and thereby to improve the phase quality of the entire image. For 5% phase noise the $B_{\perp}$ is estimated with an accuracy of 0.4 m. The methodology can be further improved by bringing additional information such as coherence image to further reduce the phase noise. In this paper, for all the calculations, the curved earth model is used.

ACKNOWLEDGEMENT

The authors are thankful to Kuwait University, Kuwait and IIT Roorkee, India for their support. Thanks are due to Mr. Pravin Kumar, CSRE, IIT Bombay for having useful discussions during the course of the work.

REFERENCES

Abdelfattah, R., Nicolas, J.M., & Boussema, M.R. 2000. Impact of orbital parameters on DEM production by SAR interferometry. IEEE Transactions. on Geoscuebce. Sec. and Remote Sensing. 2: 739-741.

Bamler, R. & Philipp H. 1998. Synthetic aperture radar interferometry. Inverse problems, **14**:R1-R55. http://www.iop.org/EJ/abstract/0266-5611/14/4/001

Bhagavath K, P. & Vishal. 2002. A model for development of a technique for accurate generation of DEM using ERS SAR Data. Technical Report, Microwave Remote Sensing Group, CSRE, Indian Institute of Technology, Bombay, India.

Christoph, R., Xia, Ye., Hermann, K., Franz-Heinrich, M., Ludger, T., Johann, B. & Michaela, F. 1996. Impact of precise orbits on SAR interferometry. Proceedings of FRINGE-96, Zurich, Switzerland http://www.geo.unizh.ch/rsl/fringe96/papers/reigber-et-al/

Franceschetti, G. & Lanari, R. 1999. Synthetic Aperture RADAR Processing. CRC Press, New York, NY, USA., 31-33.

Hanssen R. F. 2001. Radar Interferometry -- data interpretation and error analysis. Kluwer Academic Publishers, The Netherlands. ISBN 0-7923-6945-9.

Indian InSAR Group News Letter. 1999. Department of Science and Technology, Government of India, New Delhi, India. **1**: 1-15

Kumar, N. P. 2001. Application of SAR Interferometry and GPS to DEM generation and evaluation. M. Tech. project report, Department of Civil Engineering, IIT, Bombay, India.

Knedlik, S. & Loffeld, O. 2000. Analysis of different maximum aposteriori estimation approaches for parameter calibration. IEEE Transactions on Geosciences and Remote Sensing, **2**: 773-775.

Knedlik, S., Loffeld, O., Hein, A., & Arndt, C. 1999. A novel approach to accurate baseline estimation. IEEE Transactions on Geosciences and remote Sensing, **1**: 254-256.

Li, F.K. & Goldstein, R.M. 1990. Studies of multibaseline spaceborne interferometric synthetic aperture radars, IEEE Transactions on Geoscience and Remote Sensing, **28**: 88-97.

Massonnet, D., Rossi, M., Carmona, C., Adagna, F., Peltzer, G., Feigl, K. & Rabaute, T. 1993. The displacement field of the Landers earthquake mapped by radar interferometry. Nature 364 **(8):**138-142.

Massonnet, D. & Feigl, K. L. 1998. RADAR Interferometry and its application to changes in the earth's surface. Reviews of Geophysics 36(**4**) 441-500.

Prati, C. & Rocca, F. 1990. Limits to the resolution of elevation maps from stereo SAR images. Int. J. Remote Sensing 11(**12**): 2215-2235.

Prati, C., Rocca, F. & Guarnieri, A. M. 1993. SAR interferometry experiments with ERS-1. Proceedings of 1st ERS-1 Symposium, Cannes, France. 211-218.

Seymour. M. & Cumming, I. G. 1997. Calibrating interferometers with high quality DEM. International Geosciences and Remote Sensing Symposium, IGARSS'97, Singapore, August 3-8.

Small, D., Werner, C. & Nüesch, D. 1993. Baseline Modelling for ERS-1 SAR interferometry. Proceedings of IGARSS'93, Tokyo, Japan 1204-1206.

Small. D. & Nüesch. D. 1996. Validation of height model from ERS interferometry. Proceedings of FRINGE 96, Zurich, Switzerland. http://www.geo.unizh.ch/rsl/fringe96/papers/small-nuesch/

Seymour, M. S. & Cumming I. G. 1996. An iterative algorithm for ERS Baseline estimation. Proceedings of Fringe 1996, Zurich, Switzerland. http://www.geo.unizh.ch/rsl/fringe96/papers/seymour-cumming/

Singh, K., Stussi, N., Keong, K. L. & Hock, L. 1997. Baseline estimation in interferometric SAR. Proceedings of 3rd ERS Symposium, Florence, Italy. http://earth.esa.int/symposia/ers97/papers/singh/

Toutin, T. & Gray, L. 2000. State of the art of elevation extraction from satellite SAR data. ISPRS Journal of Photogrammetry and Remote Sensing, **55**: 13-33.

Wu. B. I., Pacheco. J., Grzegorczyk. T. M., Zhang. Y. & Kong. J. A. 2002. Baseline estimation for SAR Interferometry using ground control points. Proceedings of PIERS 2002. Cambridge, MASS, USA. July 1-5.

Zebker, H. A. & Villasenor J. 1992. Decorrelation in interferometric radar echoes, IEEE Transactions on Geoscience & Remote sensing, 30(**5**): 950 - 959.

Zebker, H. A. & Glodstein, R. M. 1986. Topographic mapping from interferometric synthetic aperture radar observations. Journal of Geophysical Research, **91 (B5)**: 4993-4999.

Submitted : *20/2/2006*
Revised : *1/11/2006*
Accepted : *13/11/2006*

تقنية تكرارية لتقدير متغيرات الخط الثابت في مقياس التداخل لرادار العدسة الصنعي SAR

كوتا سيفاسانكرا راو[1] و بغافاث كومارب[2] و فيشال[2] و هالة خالد أحمد الجسار[1]

[1]قسم الفيزياء – كلية العلوم – جامعة الكويت

[2]قسم الهندسة المدنية – المؤسسة الهندية للتكنولوجيا – روركي – الهند

خلاصة

الخط الثابت هو أقصر مسافة بين مساري القمر الصنعي. وهو يعتبر متغير مهم في قياس التداخل لرادار العدسة الصنعي (SAR) حيث له تأثير مباشر على دقة نموذج الارتفاعات الرّقمي (DEM) وقياسات الانحرافات السطحية الناتجة عن الانخفاضات الأرضية والزلازل وغير ذلك.

لقد تم تطوير نماذج مبسطة ودقيقة لتحديد متغيرات الخط الثابت للأرض المستوية بالإضافة للأرض المنحنية. قورنت نتائج هذه النماذج المبسطة مع نماذج أخرى مبسطة ووجد اتفاق بينها. وقدرت متغيرات الخط الثابت باستخدام طريقة نيوتن – رافسون ثم بعد ذلك استخدمت طريقة حساب المربعات الدنيا بمحاكاة 95 نقطة تحكم أرضي وزعت جيدا في كل أنحاء موقع القمر الصنعي (الارتفاعات – الأطوار).

التقنية التكرارية المقدمة في هذا البحث أوضحت بالأمثلة كيفية تحسين تقدير الخط الثابت من التشويش الطوري. وطورت معادلة التحويل لتقليل التشويش الطوري من بقية الصورة لتوليد نموذج الارتفاعات الرقمي (DEM).